ARL-TR-7898 ● DEC 2016

US Army Research Laboratory

Small-Angle X-ray Scattering (SAXS) Instrument Performance and Validation Using Silver Nanoparticles

by Frederick L Beyer

NOTICES

Disclaimers

The findings in this report are not to be construed as an official Department of the Army position unless so designated by other authorized documents.

Citation of manufacturer's or trade names does not constitute an official endorsement or approval of the use thereof.

Destroy this report when it is no longer needed. Do not return it to the originator.

ARL-TR-7898 ● DEC 2016

US Army Research Laboratory

Small-Angle X-ray Scattering (SAXS) Instrument Performance and Validation Using Silver Nanoparticles

by Frederick L Beyer
Weapons and Materials Research Directorate, ARL

REPORT DOCUMENTATION PAGE

Form Approved
OMB No. 0704-0188

1. REPORT DATE *(DD-MM-YYYY)*	2. REPORT TYPE	3. DATES COVERED (From - To)
December 2016	Technical Report	August 2016

4. TITLE AND SUBTITLE
Small-Angle X-ray Scattering (SAXS) Instrument Performance and Validation Using Silver Nanoparticles

5a. CONTRACT NUMBER

5b. GRANT NUMBER

5c. PROGRAM ELEMENT NUMBER

6. AUTHOR(S)
Frederick L Beyer

5d. PROJECT NUMBER

5e. TASK NUMBER

5f. WORK UNIT NUMBER

7. PERFORMING ORGANIZATION NAME(S) AND ADDRESS(ES)
US Army Research Laboratory
ATTN: RDRL-WMM-G
Aberdeen Proving Ground, MD 21005-5069

8. PERFORMING ORGANIZATION REPORT NUMBER
ARL-TR-7898

9. SPONSORING/MONITORING AGENCY NAME(S) AND ADDRESS(ES)

10. SPONSOR/MONITOR'S ACRONYM(S)

11. SPONSOR/MONITOR'S REPORT NUMBER(S)

12. DISTRIBUTION/AVAILABILITY STATEMENT
Approved for public release; distribution is unlimited.

13. SUPPLEMENTARY NOTES

14. ABSTRACT
Small-angle X-ray Scattering (SAXS) is a powerful technique for characterizing the morphology of certain materials but requires that great care be given to data collection, data correction, and instrumental effects on the data. In this report, the performance of the US Army Research Laboratory's new SAXS instrument is compared to the predicted performance and tested using samples of silver nanoparticles provided by an outside laboratory. The effect of beam-stop shadowing is discussed, and corrections for this effect are applied to the data.

15. SUBJECT TERMS
small-angle X-ray scattering, SAXS, nanoparticle, calibration, resolution performance

16. SECURITY CLASSIFICATION OF:			17. LIMITATION OF ABSTRACT	18. NUMBER OF PAGES	19a. NAME OF RESPONSIBLE PERSON
a. REPORT	b. ABSTRACT	c. THIS PAGE			Frederick L Beyer
Unclassified	Unclassified	Unclassified	UU	20	19b. TELEPHONE NUMBER (Include area code) 410-306-0893

Contents

List of Figures

List of Tables

1. Introduction

X-ray scattering is a nondestructive technique used to characterize the morphology of materials. A collimated beam of X-rays is transmitted through a specimen, and interactions with the matter within the sample cause some portion of the X-rays to be scattered away from the transmitted primary beam. When 2 photons having wavelength λ are scattered by features separated by a distance, d, the scattered photons are in phase only at a specific angle, 2θ. This relationship is described by Bragg's law, given as

$$n\lambda = 2d \cdot sin(2\theta). \quad (1)$$

More generally, it can be shown that over the range of scattering angles, the scattered intensity, I, is a function of the scattering vector, $\boldsymbol{q}$, where the magnitude of the scattering vector is $q = 2\pi/d$.

Traditional X-ray diffraction experiments to determine crystal structure are generally concerned with features on the size of atoms, with an upper limit of feature size of a few angstroms, therefore having $d < 5$ Å, or $q > 0.6$ Å^{-1}. These data have traditionally been reported as intensity versus scattering angle in terms of 2θ, where 2θ ranges up to tens of degrees, and are called wide-angle X-ray scattering data. Conversely, small-angle X-ray scattering (SAXS), and small-angle scattering in general, describes morphological features ranging in size from 10 Å to 100 nm, thus spanning a range of q from 0.6 Å^{-1} to 0.006 Å^{-1}. Recently, a preference has developed for reporting q in nm^{-1}, but in this manuscript, q will be given in units of Å^{-1}.

SAXS experiments are most commonly performed on "soft" materials, including polymers, proteins, and other biological and bioinspired materials.[1–3] In some materials (e.g., microphase separated block copolymers) Bragg diffraction occurs, and crystal structures can be determined simply by extracting the relative positions of the diffraction peaks.[4] However, a more typical experiment involves substantial data analysis, including least-squares fitting of structural models to the data. Detailed analysis can determine the size, shape, and orientation of scattering features. In biological systems, it is sometimes possible to calculate the electron density distribution of biological molecules in solution, allowing the general shape of the complex to be determined. When a 2-D detector is used, information about anisotropic morphologies is also available. Specific interfacial area in phase-separated or filled systems, and characteristics of those interfaces, are available through analysis of the Porod scattering invariant.[5]

Proper calibration of scattered intensity is useful in many of these situations. For a laboratory-scale instrument, where direct measurement of photon flux using ion counters is not generally feasible, calibration must be achieved by comparing experimental data to a calibrated standard. One of the most reliable standards for this purpose is vitrified "glassy" carbon, which has a Guinier knee around 0.1 $Å^{-1}$, form factor scattering at low-q that is free of interdomain effects, and very high contrast.[6,7] However, calibration using glassy carbon requires that the scattering from the same specific sample be known and assumes that the scattering behavior of the glassy carbon sample is constant over time (years). These conditions may not always be true. With the advent of X-ray collimating optics,[8] the increased photon flux in laboratory instruments now allows the scattering from pure liquids (e.g., water, or cyclohexane) to be used.[9,10] The scattered intensity from water, although very weak, can be calculated from first principles, and will be the subject of a subsequent report.

A typical SAXS experiment requires correction for X-ray absorption by the sample (transmission, T), subtraction of background scattering from the instrument and sample holder (the "empty cell" correction), detector noise and cosmic radiation background ("dark frame"), and in some cases, detector sensitivity.[11] A final correction to experimentally measured SAXS data is the correction for the effect of the beam-stop shadow. Just as with light from the sun, objects illuminated by X-ray wavelength photons cast a shadow. For most X-ray detectors in use today, the direct beam in a SAXS camera is bright enough to damage the detector and must be blocked using a beam stop. The beam stop casts a shadow on the detector surface, diminishing the scattered intensity at the lowest measurable angles. The information contained in that data, however, is often the most interesting in a SAXS experiment. To recover that information, a beam-stop shadowing factor can be calculated and applied to measured data.[9] This calculation requires the knowledge of the scattering behavior of a sample in the q range affected by the beam-stop shadow. The use of calibrated glassy carbon as a secondary intensity standard thus also allows the determination of the effect of the beam stop on the data.

In 2013, the Materials Division of the US Army Research Laboratory (ARL) purchased a Rigaku Americas, Inc., SAXS instrument ("camera"). This instrument represents a substantial improvement over the older SAXS camera in use at that time. The primary changes were the use of a brighter X-ray source, the Rigaku Micromax HF007 rotating anode X-ray generator, and the addition of a focusing optic prior to the 3-pinhole collimation system. Together these improvements improved the data collection time by a factor of between 5 and 8 times, depending on the anode bias setting, and reduced smearing in the data by monochromating the incident X-ray radiation. A further enhancement was the purchase of a 200-mm-

diameter area detector, which by virtue of its large size, allows collection in a single experiment of data spanning a wider *q*-range when placed at a comparable distance from the sample.

In the following sections, the procedure used to collect SAXS data on this new instrument will be described, including calibration using glassy carbon, as a secondary intensity standard. The geometry of the new SAXS camera will be analyzed, including determination of the beam-stop shadow on the data. Finally, scattering data collected for a dispersion of silver nanoparticles (AgNPs) will be analyzed, illustrating these procedures.

2. Experimental

2-D SAXS patterns were collected using a Rigaku SMAX-3000 camera. The X-ray source was a MicroMax-007HFM rotating copper anode operated at 40 kV and 30 mA, for a total power of 1.2 kW. The cathode produces a focal spot on the anode of 0.3 mm by 3 mm, that when observed from a take-off angle of 6° appears as a square roughly 0.3 mm by 0.3 mm. The resulting characteristic X-rays are then focused and monochromated to the K_α doublet, with wavelength (λ) of 1.5418 Å, using a Confocal Max-Flux double-focusing optic.[8] The photon beam was then shaped using an evacuated 3-pinhole collimation flight path.

The samples were characterized at a sample-to-detector distance of 1.5-m camera length using a Gabriel-type 2-D multiwire xenon proportional counter.[12] Based on the circular integration of a calibrated glassy carbon standard, the detector's effective angular range was found to be 0.01–0.25 $Å^{-1}$.[7,13] Distance and beam-center calibration were performed with silver (Ag) behenate.[14]

Two samples of AgNPs dispersed in water were obtained from Dr Brian Pauw at the BAM Federal Institute for Materials Research and Testing, Germany. The AgNP samples were loaded into 1- and 2-mm-diameter quartz capillaries (Charles Supper Company, Natick, MA, USA), which were then sealed using "5 Minute" epoxy. The epoxy was allowed to cure overnight. The samples were then placed on the sample holder and characterized in the SAXS camera. The sample chamber vacuum was approximately 75 mTorr, which has been found empirically to be sufficient for data collection with low background noise.

Raw data were corrected for sample background (empty), detector (dark field) noise, and sample absorption (transmission).[11] The isotropic 2-D data were azimuthally averaged so that 1-D I(*q*) data could be evaluated and modeled. IGOR Pro v. 6.37 (Wavemetrics, Inc.) was used for all data processing and analysis. Two sets of procedures, "Nika" and "Irena", available from the Advanced Photon

Source, Argonne National Laboratory, were used for all data handling.[15] The form factor modeling incorporated in the Irena package is based on procedures developed at the National Institute for Standards and Technology, Gaithersburg, MD.[16]

Transmission electron microscopy (TEM) data were collected using a JEOL JEM-2100F transmission electron microscope operated at 200 kV. Bright field TEM was performed on samples prepared by placing drops of AgNPs suspended in water onto TEM grids coated with lacey carbon films, ultrathin films of pure carbon, or both. The best results were obtained using grids coated with lacey carbon. Images were collecting using a 10.7-MP fiber-optically coupled charge-coupled device detector manufactured by Gatan, Inc. (Orius model 832). No additional processing was performed.

3. Results and Discussion

One of the first steps in the use of the new instrument was to determine the minimum value of the scattering vector magnitude, *q*, that could be measured. This was accomplished using a simple geometric calculation based on the 3-pinhole configuration and assuming uniform illumination across the entrance aperture (first pinhole).[9] In Table 1, PH*i* and L*i* refer to the i^{th} pinhole and the distance between pinholes *i* and *i*+1. dL_{SAM} is the distance between PH3 and the sample, while dL_{BS} is the distance between the beam stop and the plane of the detector (anode). Although every effort was made to be precise in these measurements, some information is approximate by definition, such as the distance between the beam stop and the detector, because of the nature of the multiwire detector.[12] The double-focusing optic filters out all radiation other than the $Cu_{K\alpha}$ peak, which has wavelength 1.5418 Å.

Table 1 Camera configuration information as calculated

Pinhole	Diameter (µm)	Segment	Distance (mm)	Results
PH1	400	L1	690	Sample-to-detector distance = 1525 mm
PH2	200	L2	486	α = 0.000435 radians
PH3	700	L3	1510	β = 0.000926 radians
. . .	. . .	dL_{SAM}	15	Minimum q = 0.00475 $Å^{-1}$
. . .	. . .	dL_{BS}	30	Actual minimum q = 0.00535 $Å^{-1}$

Based on the information measured and discussions with the manufacturer, the minimum value of *q* that should be achievable is 0.00535 $Å^{-1}$, corresponding to a real space dimension of 117.4 nm. This dimension includes the effect of the beam stop on resolution. The actual minimum resolution based simply on the camera geometry should be q = 0.00475 $Å^{-1}$, which falls inside the 4-mm-diameter beam

stop. Another important dimension is the diameter of the beam at the sample position, which is calculated to be 636 µm. In practice, the minimum resolution is not easily achieved. The beam stop casts a diffuse shadow on the detector, which is further expanded by the smearing effects of the multiwire detector. This shadow affects the data to a q value as high as 0.01 $Å^{-1}$. For some experiments, this effect is negligible, but for others, the lowest angle data are required. In the latter case, the effect of the beam-stop shadow can be mitigated by scaling the low angle data using a function determined from a sample with known scattering.[9]

Figure 1 gives examples of the Ag behenate beam center and distance calibration data, glassy carbon data, data from one of the AgNP samples, the empty cell data (capillary and water), and detector dark noise. In this figure, none of the data have been corrected other than to be normalized by collection time so that the relative scattering power of the different samples can be more readily observed. The strong Bragg diffraction peaks from Ag behenate are evident and demonstrate why this material is a good calibration standard. Glassy carbon scatters very strongly, and its structure does not change appreciably with time. The AgNP solution also scatters strongly, such that the corrections for background and detector noise have minimal effect on the data (which is desirable).

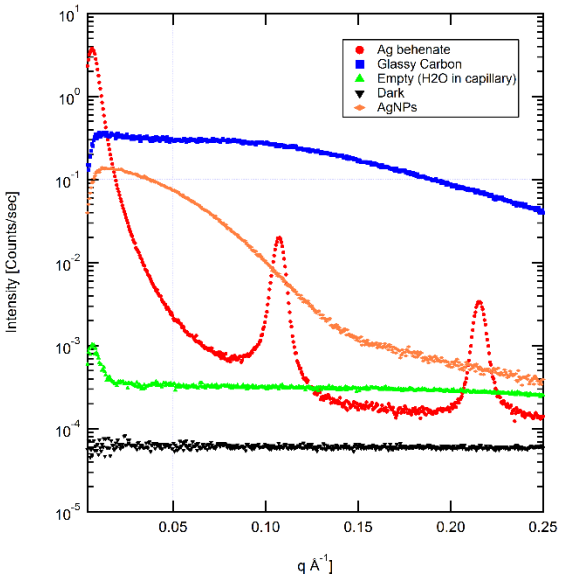

Fig. 1 Azimuthally averaged SAXS data for Ag behenate (red), glassy carbon (blue), a glass capillary containing water only (green), the detector dark noise (black), and a sample of Ag nanoparticles dispersed in water (orange). Data have been normalized by collection time only.

In Fig. 2, the effect of the beam-stop shadow is clearly evident in the glassy carbon data collected at ARL (blue). It is known that the glassy carbon scattering data should not decrease as $q \rightarrow 0$, but a clear decrease in scattered intensity is observed for $q < 0.01$ Å^{-1}. As discussed previously, this effect can be mitigated by correcting the low-q data using a function determined based on scattering from a known material. In this case, the glassy carbon sample (T4) provided by Dr Ilavsky at the Advanced Photon Source works well because the scattering from this sample is known down to $q < 0.002$ Å^{-1}. By dividing the experimental data collected at ARL by the known scattering data, a set of data (green) is generated by which the ARL data can then be normalized to correct for the beam-stop shadow. As can be seen in Fig. 2, however, this data set is somewhat noisy in the low-q regime. To compensate for this noise, the normalization data are fitted with an exponential of the form shown in Eq. 2.

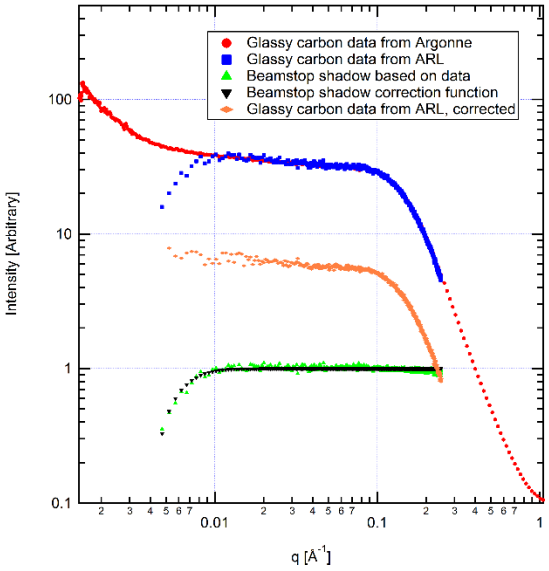

Fig. 2 Glassy carbon SAXS data from Argonne National Laboratory (red, on absolute scale, units of cm^{-1}), background-corrected data from ARL (blue, scaled to match the data from Argonne), the beam-stop shadow normalization data (green), the beam-stop shadow normalization function (black), and beam-stop shadow-corrected glassy carbon data from ARL, scaled arbitrarily for clarity

$$f(q) = y_0 + A_0 * e^{-\frac{q}{\tau}}. \quad (2)$$

The background-corrected data (blue) can then be normalized by the beam-stop shadow correction function (black), which effectively raises the intensity of the data at the very lowest q (orange).

Furthermore, after correcting for the beam-stop shadow, the apparent minimum value of q for which usable intensity is obtained was 0.00473 Å^{-1}. However, this value is within the direct footprint of the 4-mm-diameter beam stop on the plane of

the detector. Discarding the data point at the lowest q gives a minimum q of 0.00522 Å^{-1}, which is slightly better than the calculated resolution given in Table 1 (0.00535 Å^{-1}). In practice, the minimum value of q used during data reduction should therefore be chosen conservatively.

Figure 3 shows the effect of the background correction and beam-stop shadow correction on a typical set of data for a sample of Ag nanoparticles. Both corrections are important in this experiment. The scattering from the capillary (green) shows a significant upturn in the low-q region, which, if not removed from the raw data, might suggest the presence of AgNP aggregates.[17] The beam-stop shadow, however, causes a decrease in low-q intensity, mimicking the presence of interparticle scatter.[2] This would suggest that the concentration of nanoparticles is too high for accurate size analysis. The corrected data (red) show neither an upturn or decrease in intensity down to $q \approx 0.006$ Å^{-1}, confirming the presence of only well-dispersed nanoparticles.

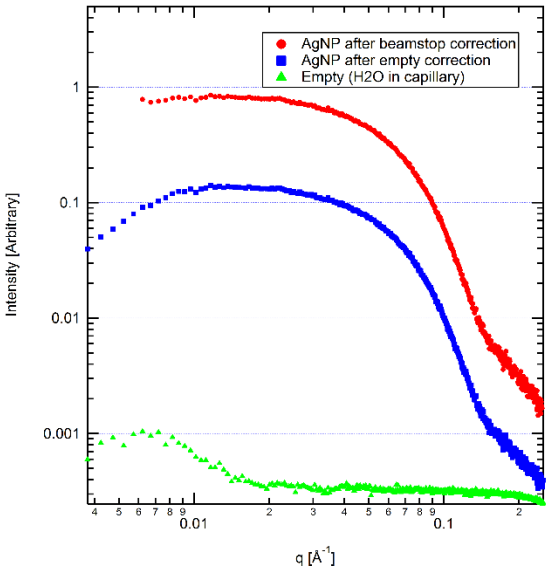

Fig. 3 SAXS data showing scattering from a water-filled capillary (green), AgNPs in a water-filled capillary after background subtraction (blue), and the same AgNP data after correction for back-stop shadowing (red)

Once the raw data have been corrected for background and the effect of beam-stop shadowing has been removed, they can be fit using the appropriate form factor for the scattering particle. In this case, the form factor for a spheroid (Eq. 3) is most appropriate, given the approximately spherical shape of AgNPs.[18]

$$P(q) = scale \cdot \left[\frac{3[\sin(qr) - qr \cdot \cos(qr)]}{(qr)^3}\right]^2 + bkgd\ . \qquad (3)$$

In this formalism, volume, *V*, is the volume of a sphere with radius *r*. The terms *scale* and *bkgd* are simply constants that account for background noise, contrast between the spherical particles and the solvent, and other instrument-related terms. For aspect ratios greater than 1.01, the calculation uses the form factor in Eq. 3 but replacing *qr* with Eq. 4:

$$qr = qr\sqrt{[1 + (AR^2 - 1)\cos^2(\theta)]}\,. \tag{4}$$

Figure 4 shows an example of a typical least-squares fit to the SAXS data using the spheroid form factor and allowing the aspect ratio to vary. The normalized residual is less than 1 for all but the lowest angle data, a fit that is quite good. If the aspect ratio is fixed at 1.0, substantial deviations between the data and the fit occur around q = 0.14 Å^{-1} as well as at the lowest angles.

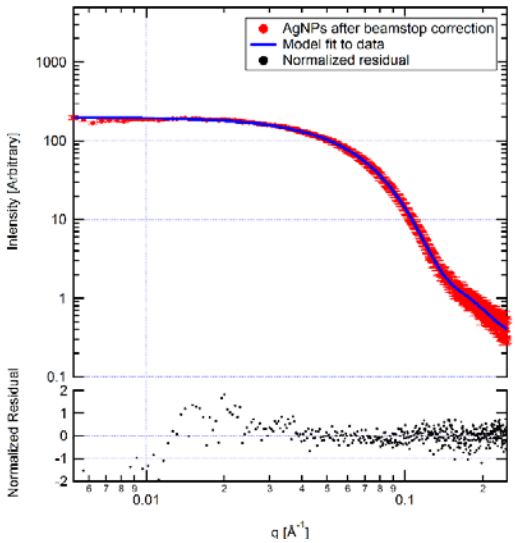

Fig. 4 Least squares fit of a spherical form factor to a typical set of data for Ag nanoparticles

Two samples were provided by Pauw, "0043" and "0045". Sample 0043 was found to have a mean particle radius of 28.60 Å, with a standard deviation of 5.21 Å and an aspect ratio of 1.42. Sample 0045 was found to have a mean particle radius of 28.67 Å, with a standard deviation of 5.29 Å, and an aspect ratio of 1.40. Pauw later revealed that each participant in the study was provided with 2 identical samples to test the reproducibility of each laboratory's data and procedures. The data from ARL and all the other laboratories were fit by Pauw using the same approach as the fitting performed at ARL and reported previously, generating a mean particle diameter (undisclosed) and a particle size distribution (also undisclosed).[19] Figure 5 shows the 2 data sets from ARL relative to data from other researchers using laboratory-scale instruments and to data from synchrotron facilities, plotted as a function of deviation from the distribution mean and from the distribution variance. In both measures, the data from ARL are excellent.

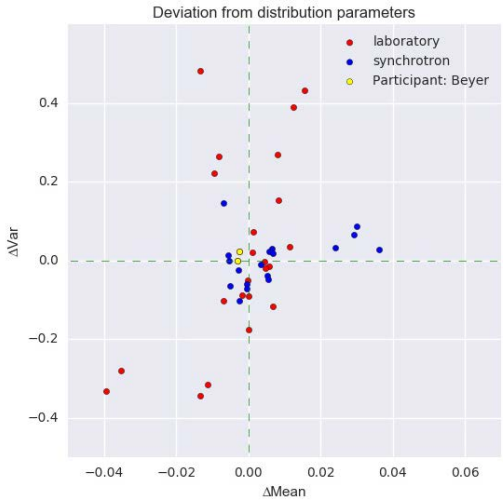

Fig. 5 Deviation from the particle size distribution mean (ΔMean) and distribution breadth (ΔVar). Data collected at ARL are shown in yellow and are very close to the center of both parameters. The scale varies between the 2 axes.[19,20]

Finally, TEM data were collected to confirm the particle size, as shown in Fig. 6. In most cases, the typical particle diameter was observed to be approximately 5–6 nm. In most micrographs collected, a small number of larger particles can be observed. These particles appear to be aggregates of 2 or more individual nanoparticles. The formation of the aggregates is most likely due to the TEM sample preparation process, which concentrates the nanoparticles on the carbon film surfaces but may also be due to aging effects on the nanoparticle dispersion, as the TEM samples were prepared 4 months after receipt of the samples. These TEM data also highlight the benefits of using SAXS for morphology analysis. SAXS provides an ensemble average over a relatively large volume as comparted to the microscopic volume characterized in TEM.

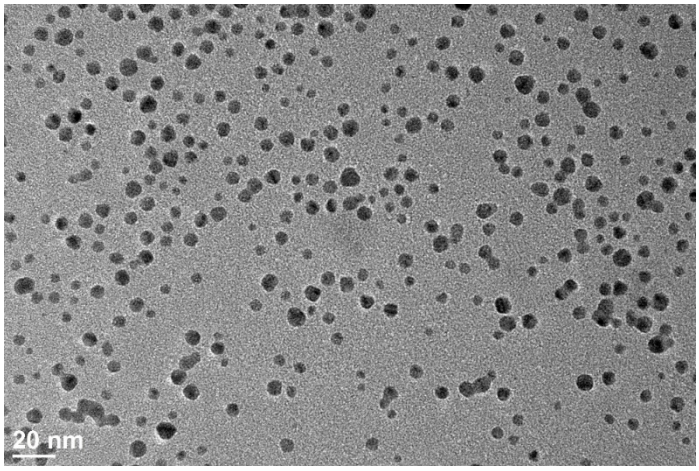

Fig. 6 TEM micrograph showing dispersed Ag nanoparticles on a carbon support film. The nanoparticles range in size from approximately 3 to 10 nm, with a few aggregates of multiple particles visible.

4. Conclusions

SAXS is a powerful tool for characterizing the internal structure of materials, but the indirect nature of the technique requires that great attention be paid to instrument calibration and data handling. Correction of the data for the effects of beam-stop shadowing has been described, and it was found that the instrument has a slightly larger resolution (lower minimum q) than anticipated based on a simple geometric model. Two samples of AgNPs dispersed in water were characterized using these techniques. The 2 nanoparticle samples were found to be essentially identical, with a mean particle diameter of 5.6 nm. Furthermore, it was found that the data collected using the ARL instrument are among the best data available, including that from synchrotron sources, confirming the accuracy of the data handling and calibration procedures in use at ARL.

5. References

1. Glatter O, Kratky O. Small angle X-ray scattering. New York (NY): Academic Press; 1982.
2. Roe R-J. Methods of X-ray and neutron scattering in polymer science. New York (NY): Oxford University Press; 2000.
3. Strobl G. The physics of polymers: concepts for understanding their structures and behavior. 3rd ed. Berlin Heidelberg (Germany): Springer; 2006.
4. Hamley IW. The physics of block copolymers. 1st ed. New York (NY): Oxford University Press; 1998. p. 424.
5. Bonart R, Muller EH. Phase separation in urethane elastomers as judged by low-angle x-ray-scattering. 1. Fundamentals. Journal of Macromolecular Science-Physics B. 1974;10:177–189.
6. Russell TP, Lin JS, Spooner S, Wignall GD. Intercalibration of small-angle X-Ray and neutron-scattering data. Journal of Applied Crystallography. 1988;21:629–638.
7. Zhang F, Ilavsky J, Long GG, Quintana JPG, Allen AJ, Jemian PR. Glassy carbon as an absolute intensity calibration standard for small-angle scattering. Metallurgical and Materials Transactions A. 2009;41:1151–1158.
8. Kusz J, Bohm H. Performance of a confocal multilayer X-ray optic. Journal of Applied Crystallography. 2002;35:8–12.
9. Pedersen JS. A flux- and background-optimized version of the NanoSTAR small-angle X-ray scattering camera for solution scattering. Journal of Applied Crystallography. 2004;37:369–380.
10. Orthaber D, Bergmann A, Glatter O. SAXS experiments on absolute scale with Kratky systems using water as a secondary standard. Journal of Applied Crystallography. 2000;33:218–225.
11. Richard PB. Everything SAXS: small-angle scattering pattern collection and correction. Journal of Physics: Condensed Matter. 2013;25:383201.
12. Petrascu AM, Koch MHJ, Gabriel A. A beginners' guide to gas-filled proportional detectors with delay line readout. Journal of Macromolecular Science-Physics. 1998;B37:463–483.

13. Dreiss CA, Jack KS, Parker AP. On the absolute calibration of bench-top small-angle X-ray scattering instruments: a comparison of different standard methods. Journal of Applied Crystallography. 2006;39:32–38.

14. Huang TC, Toraya H, Blanton TN, Wu Y. X-ray-powder diffraction analysis of silver behenate, a possible low-angle diffraction standard. Journal of Applied Crystallography. 1993;26:180–184.

15. Ilavsky J, Jemian PR. Irena: tool suite for modeling and analysis of small-angle scattering. Journal of Applied Crystallography. 2009;42:347–353.

16. Kline SR. Reduction and analysis of SANS and USANS data using IGOR Pro. Journal of Applied Crystallography. 2006;39:895–900.

17. Kane MC, Londono JD, Beyer FL, Brennan AB. Characterization of the hierarchical structures of a dry nanopowder in a polymer matrix by X-ray scattering techniques. Journal of Applied Crystallography. 2009;42:925–931.

18. Guinier A, Fournet G. Small-angle scattering of X-rays. New York (NY): John Wiley and Sons; 1955.

19. Pauw BR. Looking at nothing: a weblog about small-angle scattering; 2016 [accessed 2016 NOV 23]. http://www.lookingatnothing.com/index.php/archives/2101.

20. Pauw BR. BAM Federal Institute for Materials Research and Testing, Germany. Email communication, 2016 Nov 18.

List of Symbols, Abbreviations, and Acronyms

1-/2-D	1-/2-dimensional
AgNP	silver nanoparticle
ARL	US Army Research Laboratory
SAXS	small-angle X-ray scattering
TEM	transmission electron microscopy

1 (PDF)	DEFENSE TECHNICAL INFORMATION CTR DTIC OCA
2 (PDF)	DIRECTOR US ARMY RESEARCH LAB RDRL CIO L IMAL HRA MAIL & RECORDS MGMT
1 (PDF)	GOVT PRINTG OFC A MALHOTRA
1 (PDF)	DIR USARL RDRL WMM G F BEYER